ATLAS NOTE

ATLAS-CONF-2012-106

August 10, 2012

Search for scalar bottom pair production in final states with missing transverse momentum and two b-jets in pp collisions at $\sqrt{s}$=7 TeV with the ATLAS Detector

The ATLAS Collaboration

Abstract

The results of a search for pair production of the scalar partners of the bottom quarks in 4.7 fb^{-1} of pp collisions at $\sqrt{s} = 7$ TeV using the ATLAS detector at the LHC are reported. Scalar bottoms are searched for in events with large missing transverse momentum and two jets identified as originating from a b-quark in the final state. Results are interpreted in a R-parity conserving minimal supersymmetric scenario, assuming that the scalar bottom decays exclusively into a bottom quark and a neutralino. Scalar bottom masses up to 490 GeV are excluded for $m_{\tilde{\chi}_1^0} = 0$ at 95% confidence level. Neutralino masses up to 180 GeV are excluded for scalar bottom masses around 400 GeV. The present limits significantly extend previous results.

1 Introduction

Supersymmetry (SUSY) [1–9] provides an extension of the Standard Model (SM) which resolves the hierarchy problem [10–13] by introducing supersymmetric partners of the known bosons and fermions. In the framework of the R-parity conserving minimal supersymmetric extension of the SM (MSSM) [14–18], SUSY particles are produced in pairs and the lightest supersymmetric particle (LSP) is stable, providing a possible candidate for dark matter. In a large variety of models, the LSP is the lightest neutralino ($\tilde{\chi}_1^0$). The coloured superpartners of quarks and gluons, the scalar quarks (squarks, $\tilde{q}$) and gluinos ($\tilde{g}$), if not too heavy, would be produced in strong interaction processes at the Large Hadron Collider (LHC) and decay via cascades ending with the LSP. The undetected LSP results in missing transverse momentum –whose magnitude is referred to as $E_{\mathrm{T}}^{\mathrm{miss}}$ – while the rest of the cascade yields final states with multiple jets and possibly leptons. In the MSSM, the scalar partners of right-handed and left-handed quarks, $\tilde{q}_R$ and $\tilde{q}_L$, can mix to form two mass eigenstates. The mixing depends on the corresponding quark Yukawa coupling and so is largest for the third generation squarks. Large mixing can yield scalar bottom ($\tilde{b}_1$) and top ($\tilde{t}_1$) mass eigenstates which are significantly lighter than other squarks. Consequently, $\tilde{b}_1$ and $\tilde{t}_1$ could be produced with large cross sections at the Large Hadron Collider (LHC).

This paper extends the search for direct $\tilde{b}_1$ pair production at ATLAS presented in Ref. [19], which used 2.05 fb^{-1} of data collected in the first half of 2011 at a centre-of-mass energy of 7 TeV. A SUSY particle mass hierarchy such that the scalar bottom (referred to as sbottom, in the following) decays exclusively via $\tilde{b}_1 \to b\tilde{\chi}_1^0$ is assumed. The present analysis comprises the full 2011 dataset of 4.7 fb^{-1} and adopts improved selections to enhance the sensitivity across the sbottom-neutralino mass plane.

2 General analysis strategy

The signal of interest of this analysis is sbottom pair production, with the decay of the sbottom into a b-quark and a neutralino, which is the LSP. The final state consists of two b-jets and transverse missing momentum (due to the two LSPs going undetected). No isolated leptons are produced in the final state; thus the analysis relies on a missing transverse momentum trigger. The dominant SM background processes are expected to be events with large missing transverse momentum from neutrino production, through the decay of a W boson in association with a lepton or via a $Z \to \nu\nu$ decay. Exploiting the presence of b-jets in the final state strongly reduces direct W and Z production, favouring the selection of $t\bar{t}$ production, where at least one top quark decays leptonically.

The parameter that drives the kinematics of the final state is the separation in mass between the sbottom and the neutralino, $\Delta m = m_{\tilde{b}_1} - m_{\tilde{\chi}_1^0}$. If Δm is large, then the two b-jets have significant transverse momentum (p_{T}). The top pair production background can be reduced by making use of a variable which plays a role equivalent to the transverse mass in the W decay, the contransverse mass between the two b-jets (see Appendix A). This variable has a well defined kinematical end-point for top pair production background.

For smaller values of Δm, the rejection power of the contransverse mass decreases, and different strategies have to be used. In this case, the presence of a high p_{T} jet from initial state radiation recoiling against the sbottom pair system can be exploited.

The background estimation is based on the definition of control regions with a kinematic selection closely mimicking that of the signal regions, but requiring either one or two isolated leptons. The 1-lepton control region is sensitive to top production. The 2-lepton control region

is sensitive either to Z production (in the di-lepton mass peak) or to top production (in the sidebands of the Z peak). The normalisations of these two background processes are obtained with a combined likelihood fit in the control regions.

3 Monte Carlo simulation

Samples of simulated events are used for the description of the background and to model the SUSY signal. Monte Carlo (MC) samples for top quark pair and single top production are simulated with MC@NLO [20, 21], fixing the top quark mass at 172.5 GeV, and the next-to-leading-order (NLO) parton density function (PDF) set CT10 [22]. Samples of W+jets, Z+jets are generated with ALPGEN [23] and PDF set CTEQ6L1 [24]. Dedicated samples of W/Z plus heavy flavour jets are included in the analysis, after taking care of possible overlaps with the inclusive samples. The fragmentation and hadronisation for the ALPGEN and MC@NLO samples are performed with HERWIG [25], using JIMMY [26] for the underlying event. Samples of $t\bar{t}+b\bar{b}$ events have been generated with ALPGEN, while samples of $t\bar{t}$+W and $t\bar{t}$+Z events are generated with MadGraph [27] interfaced to PYTHIA [28]. Diboson + jets (WW, WZ, ZZ) samples are generated with SHERPA [29]. For the comparison with data, all SM background cross sections are normalised to the results of higher-order calculations when available. The W and Z/γ^* production processes are normalised to the next-to-next-to-leading order (NNLO) cross sections while the $t\bar{t}$ and single top production are normalised to the NLO+NNLL (next-to-next-to-leading logarithms) cross section. The cross section used for the Wbb sample is a factor of 1.15 higher than the NLO calculation, to obtain better agreement with a measurement in a dedicated control region [30].

The normalisation of the diboson production is based on cross sections determined at NLO using MCFM [31, 32]. The $t\bar{t}$ production in association with W/Z are normalised to NLO cross sections [33, 34].

The signal samples are generated using the HERWIG++ [35] v2.4.2 MC program. Signal cross sections are calculated to NLO in the strong coupling constant, adding the resummation of soft gluon emission at next-to-leading-logarithmic accuracy (NLO+ NLL) [36–38]. The nominal cross section and the uncertainty are taken from an envelope of cross section predictions using different PDF sets and factorisation and renormalisation scales, as described in Ref. [39].

The MC samples are produced using parameters tuned as described in Ref. [40, 41] and are processed through a detector simulation [42] based on GEANT4 [43]. The effect of multiple pp interactions per bunch crossing is also simulated.

4 Object reconstruction

The ATLAS detector is described in detail in Ref. [44]. It comprises an inner detector (ID) surrounded by a thin superconducting solenoid, a calorimeter system and an extensive muon spectrometer (MS) embedded in a toroidal magnetic field.

Electron candidates are reconstructed from energy clusters in the electromagnetic calorimeters matched to a track in the ID. They are required to have $p_{\mathrm{T}} > 20$ GeV, $|\eta| < 2.47$ and to pass the "medium" shower shape and track selection criteria of Ref. [45]. Tight electrons, used for the control regions, are selected using "tight" criteria, $p_{\mathrm{T}} > 20$ GeV, and with the isolation requirement that the total track momentum in a cone of $\Delta R < 0.2$ around the candidate be less than 10% of the reconstructed p_{T}.

Muons are reconstructed using an algorithm [46] that combines information from the ID and MS. Candidate muons are required to have $p_{\mathrm{T}} > 10$ GeV, $|\eta| < 2.4$, and be reconstructed with a sufficient number of hits in the ID. Tight muons are required to have $p_{\mathrm{T}} > 20$ GeV and less than 1.8 GeV in a cone of $\Delta R < 0.2$ around the candidate. In order to reject muons originating from cosmic rays, events containing muon candidates with a distance of closest approach greater than 1 mm to the hard scatter vertex in the z direction, or a transverse impact parameter greater than 0.2 mm, are rejected. The hard scatter vertex is defined as the primary vertex with the highest summed track p_{T}^2 (with track $p_{\mathrm{T}} > 0.4$ GeV).

Jet candidates are reconstructed using the anti-k_t jet clustering algorithm [47] with a distance parameter of $R = 0.4$. The measured jet energy is corrected for inhomogeneities and for the non-compensating nature of the calorimeter using p_{T}- and η-dependent correction factors based on MC results with corrections from in-situ measurements [48,49]. Furthermore, the reconstructed jet's p_{T} and η values are modified such that its direction points to the hard scatter vertex and events containing jets likely to have arisen from detector noise or cosmic rays are rejected [50]. Only jet candidates with corrected transverse momenta $p_{\mathrm{T}} > 20$ GeV and $|\eta| < 4.5$ are retained. Events are also rejected if there is any selected jet with $|\eta| < 2$ having a ratio between the scalar sum of the transverse momenta of the tracks associated with the jet divided by the jet p_{T} of less than 5%.

Following object reconstruction, candidate jets and leptons may point to the same energy deposits in the calorimeter. These overlaps are resolved by first discarding any jet candidates within $\Delta R < 0.2$ of an electron. Then, any electron or muon candidate remaining within $\Delta R < 0.4$ of any surviving jet is also discarded.

The two-dimensional missing transverse momentum vector, $\mathbf{p}_{\mathrm{T}}^{\mathrm{miss}}$, and its magnitude $E_{\mathrm{T}}^{\mathrm{miss}}$, are computed from the negative of the vector sum p_{T} of the candidate electrons, muons and jets, and all calorimeter clusters with $|\eta| < 4.9$ not associated with such objects.

After overlap removal, jets are further required to lie within $|\eta| < 2.8$. Events containing electrons or muons are rejected for the signal regions. For the 1- and 2-lepton control regions, additional quality and isolation requirements are placed on the leptons. Electrons must additionally pass the "tight" electron criteria of Ref. [45], and be isolated such that the scalar p_{T} sum of tracks within a cone of $\Delta R < 0.2$ around the electron candidate (not including the electron track) must be less than 10% of the electron p_{T}. Muons must also be isolated such that the p_{T} sum of tracks (not including the muon track) within $\Delta R < 0.2$ is less than 1.8 GeV.

A neural network based algorithm (known as MV1 [51]) is used to identify jets containing a b-hadron decay (b-jets). This uses as inputs the output weights of different algorithms exploiting the impact parameter of the inner detector tracks, the secondary vertex reconstruction and the topology of b- and c-hadron decays inside the jet. The operating point of the algorithm is chosen such that a tagging efficiency of 60% ($< 1\%$) is achieved for b-jets (light flavour or gluon jets) in $t\bar{t}$ events in MC simulation [51–53]. The b-jets are identified within the nominal acceptance of the inner detector ($|\eta| < 2.5$) and are required to have $p_{\mathrm{T}} > 30$ GeV.

5 Event selection

After the application of beam, detector, and data-quality requirements, the total luminosity considered corresponds to $\int L\mathrm{d}t = 4.7$ fb^{-1}. Events are selected using a trigger based on a $E_{\mathrm{T}}^{\mathrm{miss}}$ selection, which is found to be 99% efficient for events with $E_{\mathrm{T}}^{\mathrm{miss}}$ above 150 GeV. The triggering efficiency variations due to the data-taking periods or the pileup conditions are measured to be within 1% after the above requirements. For the 1- and 2-lepton control regions, events are required to pass the unprescaled single lepton trigger with lowest available thresh-

old in each data period. The presence of at least one primary vertex (with at least five attached tracks with $p_{\mathrm{T}} > 0.4$ GeV) is required.

A number of event-level variables has been proven to be effective in rejecting the SM background while efficiently selecting candidate sbottom pair production events. They are summarised in Appendix A.

Three sets of signal regions are defined to provide sensitivity to the different kinematic topologies associated to differing mass-splittings Δm between the sbottom and the neutralino mass.

Signal region 1 (SR1) targets signal events with large Δm, identifying the two leading jets as the sbottom decay products. A veto on a third jet with $p_{\mathrm{T}} > 50$ GeV is imposed, and the two leading jets are required to be b-tagged. The multi-jet background is heavily suppressed by selecting events with large $\Delta\phi_{\mathrm{min}}$ and $E_{\mathrm{T}}^{\mathrm{miss}}/\mathrm{m_{eff}}$. The final selection is done by applying three different thresholds on the boost-corrected contransverse mass, m_{CT}.

Signal region 2 (SR2) targets signal events with moderate Δm. Due to the softer kinematics in this region, the thresholds on the leading jet p_{T} and on m_{CT} are relaxed. A final upper cut on the additional hadronic activity in the event, $H_{\mathrm{T},2}$, is applied.

Signal region 3 (SR3) is defined to enhance sensitivity in the low Δm region by explicitly selecting final state events with a high p_{T} jet produced as initial state radiation recoiling against the sbottom pair system. High thresholds on the leading jet and on the missing transverse momentum, which are required to be almost back-to-back in ϕ, are imposed. Two additional soft jets are required to be b-tagged. As for SR1 and SR2, the multi-jet background is suppressed with appropriate selections on $\Delta\phi_{\mathrm{min}}$ and $E_{\mathrm{T}}^{\mathrm{miss}}/\mathrm{m_{eff}}$. A final upper cut on the additional hadronic activity in the event, $H_{\mathrm{T},3}$, completes the selection for SR3a. A second signal region named SR3b is defined by further increasing the thresholds on the leading jet and $E_{\mathrm{T}}^{\mathrm{miss}}$.

The definition of all signal regions is summarised in Table 1.

6 Background estimation

The dominant SM background processes in the signal regions are top and $W + \mathrm{hf}$ (hf = heavy flavour) production (where a charged lepton is produced but it is not vetoed, either because it is a hadronically decaying τ, or because it is an electron or muon out of acceptance or not reconstructed), $Z(\rightarrow \nu\bar{\nu})$+hf and multi-jet production from QCD processes. The sub-dominant background contribution from dibosons, $t\bar{t} + W/Z$ and $t\bar{t} + b\bar{b}$ is estimated using MC simulation (referred to as "Others" in the following).

The multi-jet production is estimated with a fully data-driven procedure, which consists in smearing the jet response of low-$E_{\mathrm{T}}^{\mathrm{miss}}$ seed events. The gaussian core of the jet response function is obtained from well reconstructed di-jet events, while the non-gaussian tails are obtained from three-jet events, where the missing transverse momentum can be unambiguously associated to the mis-measurement of one of the jets [54].

For each signal region, the contributions from top production (single top production is added to the $t\bar{t}$ production with a relative normalisation corresponding to that predicted by the MC) and Z+hf production are estimated simultaneously with a profile likelihood fit to two control regions.

The control regions are defined by explicitly requiring the presence of leptons in the final state[1] and other kinematic selections mimicking the ones of the corresponding SR. The set of

[1]This ensures no signal contamination from the signal of interest. Moreover, the further kinematical constraints on the control regions ensure small signal contamination also from other possible SUSY processes.

Cut	Description	Signal region			
		SR1	SR2	SR3a	SR3b
1	Trigger	$E_{\mathrm{T}}^{\mathrm{miss}}$ trigger $>$ 99% efficient for $E_{\mathrm{T}}^{\mathrm{miss}} > 150$ GeV			
2	Event cleaning	Common to all SR			
3	Lepton veto	No e/μ after overlap removal with $p_{\mathrm{T}} > 20/10$ GeV.			
4	$E_{\mathrm{T}}^{\mathrm{miss}}$	> 150 GeV	> 200 GeV	> 150 GeV	> 250 GeV
5	Leading jet $p_{\mathrm{T}}(j_1)$	> 130 GeV, $\lvert\eta\rvert < 2.8$	> 60 GeV, $\lvert\eta\rvert < 2.8$	> 130 GeV, $\lvert\eta\rvert < 2.8$	> 150 GeV, $\lvert\eta\rvert < 2.8$
6	Second jet $p_{\mathrm{T}}(j_2)$	> 50 GeV, $\lvert\eta\rvert < 2.8$	> 60 GeV, $\lvert\eta\rvert < 2.8$	> 30 GeV, $\lvert\eta\rvert < 2.8$	
7	Third jet $p_{\mathrm{T}}(j_3)$	veto if > 50 GeV, $\lvert\eta\rvert < 2.8$		> 30 GeV, $\lvert\eta\rvert < 2.8$	
8	$\Delta\phi(E_{\mathrm{T}}^{\mathrm{miss}}, j_1)$	-		> 2.5	
9	b-jet multiplicity	leading 2 jets ($p_{\mathrm{T}} > 50$ GeV, $\lvert\eta\rvert < 2.5$)		2nd- and 3rd-leading jets ($p_{\mathrm{T}} > 30$ GeV, $\lvert\eta\rvert < 2.5$)	
		$n_{b\text{-jets}} = 2$			
10	Leading b-jet p_{T}	-		< 110 GeV	
11	$\Delta\phi_{\mathrm{min}}(n)$	> 0.4 ($n = 2$)		> 0.4 ($n = 3$)	
12	$E_{\mathrm{T}}^{\mathrm{miss}}/\mathrm{m}_{\mathrm{eff}}(j_1, j_2, j_3)$	> 0.25			
13	m_{CT}	> 150, 200, 250 GeV	> 100 GeV	-	
14	$H_{\mathrm{T},x}$	-	< 50 GeV, $x = 2$	< 50 GeV, $x = 3$	

Table 1: Summary of the event selection in each signal region.

CR1L_SR1	CR2L_SR1
1 tight electron or muon	ee or $\mu\mu$
two reconstructed jets (veto on 3rd jet with $p_{\mathrm{T}} > 50$ GeV):	
$p_{\mathrm{T}}(j_1) > 130$ GeV and $p_{\mathrm{T}}(j_2) > 50$ GeV	$p_{\mathrm{T}}(j_1) > 50$ GeV and $p_{\mathrm{T}}(j_2) > 50$ GeV
$E_{\mathrm{T}}^{\mathrm{miss}} > 90$ GeV	$E_{\mathrm{T}}^{\mathrm{miss}}$ (lepton-corrected) > 90 GeV
two reconstructed b-jets (leading jets)	
40 GeV $< \mathrm{m}_{\mathrm{T}} <$ 100 GeV	40 GeV $< m_{ll} <$ 140 GeV

Table 2: Definition of the control regions adopted for SR1.

CR1L_SR2	CR2L_SR2
1 tight electron or muon	ee or $\mu\mu$
two reconstructed jets (veto on 3rd jet with $p_{\mathrm{T}} > 50$ GeV):	
$p_{\mathrm{T}}(j_1) > 60$ GeV and $p_{\mathrm{T}}(j_2) > 60$ GeV	$p_{\mathrm{T}}(j_1) > 50$ GeV and $p_{\mathrm{T}}(j_2) > 50$ GeV
$E_{\mathrm{T}}^{\mathrm{miss}} > 120$ GeV	$E_{\mathrm{T}}^{\mathrm{miss}}$ (lepton-corrected)> 90 GeV
two reconstructed b-jets (leading jets)	
40 GeV $< \mathrm{m_T} <$ 100 GeV	40 GeV $< m_{ll} <$ 140 GeV

Table 3: Definition of the control regions adopted for SR2.

CR1L_SR3	CR2L_SR3
1 tight electron or muon	ee or $\mu\mu$
three reconstructed jets	
$p_{\mathrm{T}}(j_1) > 130$ GeV	$p_{\mathrm{T}}(j_1) > 50$ GeV
$E_{\mathrm{T}}^{\mathrm{miss}} > 120$ GeV	$E_{\mathrm{T}}^{\mathrm{miss}}$ (lepton-corrected)> 90 GeV
leading jet not-tagged, 2nd and 3rd b-tagged < 110 GeV	
40 GeV $< \mathrm{m_T} <$ 100 GeV	40 GeV $< m_{ll} <$ 140 GeV

Table 4: Definition of the control regions adopted for SR3.

control regions with exactly one lepton (e, μ) in the final state and 40 GeV $< m_T <$ 100 GeV provides a data sample largely dominated by top and, to a lesser extent, W production. In the following, they are labelled as CR1L_SRX, where X=1,2,3. A set of same-flavour opposite-sign 2-lepton control regions provides a data sample dominated by Z and top production. Each region is subdivided in three bins of the di-lepton invariant mass m_{ll}, with the central bin centred around the nominal Z mass (75 GeV $< m_{ll} <$ 105 GeV). For the 2-lepton control regions, the p_T of the leptons is added vectorially to the E_T^{miss} to mimick the expected missing transverse momentum spectrum of $Z \to \nu\bar{\nu}$ events. In the following, they are labelled as CR2L_SRX, where X=1,2,3. The exact definition of each control region can be found in Tables 2, 3 and 4. The distribution of the transverse mass m_T in the 1-lepton control region (before the upper selection on m_T) and of the di-lepton invariant mass m_{ll} in the 2-lepton control region are shown in Figure 1 (for SR1) and in Figure 2 (for SR3) before the fit.

The extrapolation of the SM background to the signal region is performed with a fit based on the profile likelihood method [55]. The free parameters of the likelihood fit are the top and the Z+jets overall normalisation scales, while the contributions from all other background processes are fixed at the expected value[2]. Systematic uncertainties are treated as nuisance parameters constrained with gaussian functions and correlations are taken into account. The likelihood function is built as the product of Poisson probability density functions, describing the observed and expected number of events in the control and (when excluding SUSY models) signal regions, and the constraints on the nuisance parameters.

The reliability of the MC extrapolation of the SM background estimation is checked in several validation regions. The first set of validation regions is defined with the same kinematic selection of the control regions but with the requirement of one b-tag only. They are used to verify the stability of the b-tagging selection. A second set of 0-lepton validation regions is defined with an identical selection to the signal regions, but reversing one of the cuts: a selection on $m_{CT} < 100$ GeV is required for the validation region of SR1 and SR2, while the selection on $H_{T,3}$ has been reversed ($H_{T,3} > 50$ GeV) for the validation region of SR3. Good agreement between the fit results and the number of observed events in the validation regions is found in all cases.

The fit results in the control and in the 0-lepton validation region are summarised in Table 5 for SR1. Similar results have been obtained for the control and validation regions of the other signal regions. The net effect of the fit is to significantly increase the MC estimates of the contribution from Z production in association with heavy flavour jets in the control and signal regions, while leaving the top production normalisation basically unaffected.

7 Systematic uncertainties

The dominant detector-related systematic effects are due to the uncertainty on the tagging efficiency for b-jets and light and gluon-jets (referred to as mistag rate), and to the jet energy scale (JES) and resolution (JER) uncertainties.

The b-tagging efficiency and mistag rate have been determined by combining different methods based on the p_T spectrum of the muon relative to that of the jet in semileptonic heavy flavour hadron decays and on heavy flavour tagging in multi-jet events [51–53]. The b-tagging efficiency uncertainties are p_T- and $\eta-$ dependent. They amount, on average, to 10–20% per b-jet, with the largest uncertainties for high p_T jets, and are the dominant source of uncertainty in this analysis.

[2]The contribution of fake lepton background to the control regions has been estimated with a matrix method [45,56] and found to be negligible.

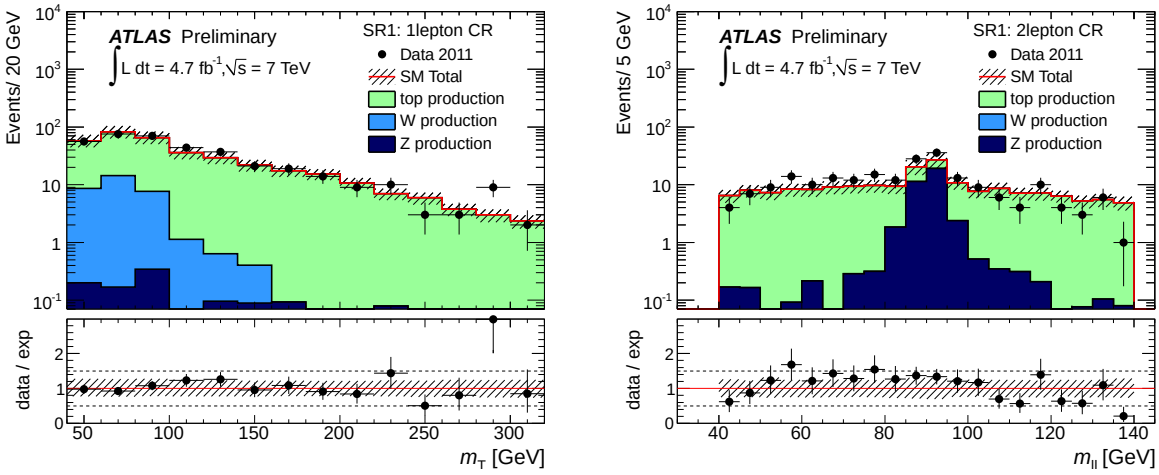

Figure 1: Left: Transverse mass distribution between the lepton and the $E_{\mathrm{T}}^{\mathrm{miss}}$ in CR1L_SR1 (before the upper selection on m_{T}) for the 1-lepton channel. Right: di-lepton invariant mass distribution in CR2L_SR1 for the 2-lepton channel. The shaded band includes both detector and theoretical systematic uncertainties. The SM prediction is normalised according to the MC expectations.

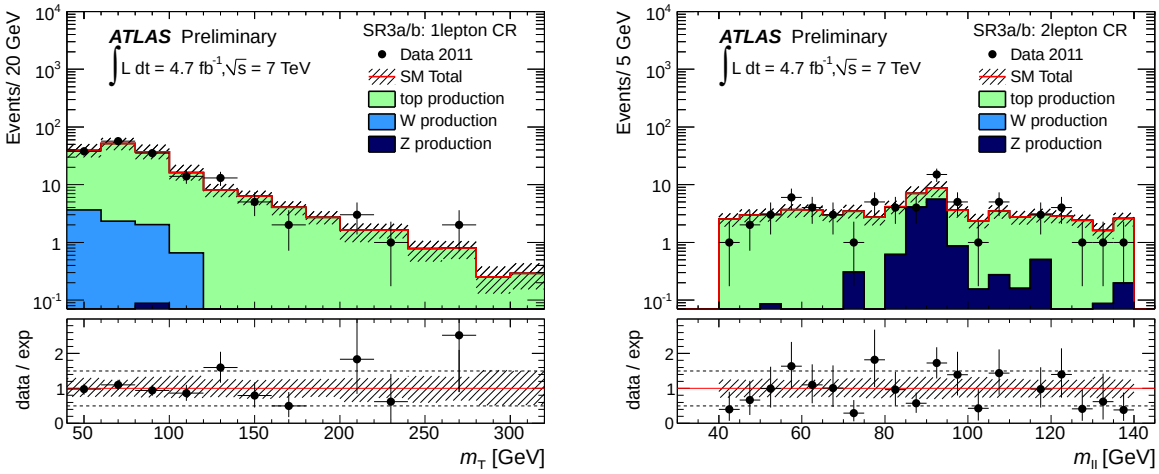

Figure 2: Left: transverse mass distribution between the lepton and the $E_{\mathrm{T}}^{\mathrm{miss}}$ in CR1L_SR3 (before the upper selection on m_{T}) for the 1-lepton channel. Right: di-lepton invariant mass distribution in CR2L_SR3 for the 2-lepton channel. The shaded band includes both detector and theoretical systematic uncertainties. The SM prediction is normalised according to the MC expectations.

channel	CR1L_SR1	CR2L_SR1	0-lepton validation
Observed events	202	211	57
Fitted bkg events	205 ± 15	209 ± 16	48 ± 7
Fitted Top events	167 ± 16	143 ± 16	34 ± 6
Fitted Z events	1.2 ± 0.4	63 ± 14	11 ± 3
Fitted W events	31 ± 17	0	3 ± 1
Fitted Others events	5.9 ± 1.4	2.6 ± 0.5	0.21 ± 0.06
Fitted multijet events	0	0	0.7 ± 0.7
MC exp. SM events	210	178	45
MC exp. Top events	173	138	35
MC exp. Z events	0.7	37	7
MC exp. W events	30	0	2.5
MC exp. Others events	6.8	2.9	0.2
exp. multijet events	0	0	0.7

Table 5: Results of the fit for the control regions and 0-lepton validation region (defined as $m_{\mathrm{CT}} < 100$ GeV) adopted for SR1.

The JES uncertainty has been derived from a combination of simulations, test beam data and in-situ measurements [50] and includes additional uncertainties arising from the event topology, the jet flavour and pile-up subtraction. Uncertainties on the JER are obtained with an in-situ measurement of the jet response asymmetry in di-jet events [57]. The JES uncertainty is dominant over the JER, and its effect is found to be between 10% and 20% depending on the signal region.

All final state object uncertainties are propagated to the $E_{\mathrm{T}}^{\mathrm{miss}}$. Additional uncertainties related to pileup contributions and calorimeter cluster energy scale uncertainties affect the component of the $E_{\mathrm{T}}^{\mathrm{miss}}$ which is associated to energy clusters not used in the reconstruction of any final state object. They have been taken into account both in the signal and control regions, although their contribution is significantly smaller ($< 5\%$) than that of the other detector uncertainties.

Additional uncertainties related to the lepton identification and energy scale have evaluated and found to be negligible.

Theory uncertainties can affect the relative population of the signal and control regions, and, therefore, the results of the fit. Concerning the top component, uncertainties on the choice of the generator have been addressed by comparing the `MC@NLO +HERWIG/JIMMY` distributions in the relevant variables used in the analysis with those obtained with the alternative NLO simulation (`POWHEG`) using the same parton shower Monte Carlo. Uncertainties on the parton shower itself have been obtained from the comparison of the mentioned `POWHEG` sample with a `POWHEG` sample using `PYTHIA` as parton shower. Finally, the uncertainty due to initial and final state radiation (ISR/FSR) is assessed using `AcerMC` samples with variations of `PYTHIA` parameters related to the ISR branching phase-space and the FSR low-p_{T} cutoff. These variations are chosen to produce jet activity in $t\bar{t}$ events that is consistent with the data [58, 59]. The total theoretical uncertainties vary between 10% and 15% depending on the signal regions (largest for the highest m_{CT} SR). The W and Z simulation is by default performed using `ALPGEN`. Theory uncertainties have been addressed by comparing different `ALPGEN` simulation samples obtained by changing the choice for the functional form and absolute value of the renormalisation and factorisation scales, and with different choices of the matching parameters. Additional

channel	SR1			SR2	SR3	
	$m_{CT} > 150$ GeV	$m_{CT} > 200$ GeV	$m_{CT} > 250$ GeV		SR3a	SR3 b
Observed	62	27	4	20	86	7
Fitted bkg	56 ± 11	24.9 ± 5.8	6.9 ± 2.3	27 ± 7	81 ± 14	8.0 ± 2.7
Fitted Top	13 ± 3	5 ± 1	1.5 ± 0.5	4.8 ± 1.2	47.8 ± 9.5	4.1 ± 1.2
Fitted Z	35 ± 10	16 ± 5	4.1 ± 1.7	17 ± 6	11.1 ± 4.5	1.3 ± 0.9
Fitted W	6.2 ± 3.8	2.3 ± 1.1	0.8 ± 0.6	3.1 ± 1.5	13 ± 8	2.4 ± 2.0
Fitted Others	2.2 ± 0.6	1.2 ± 0.4	0.5 ± 0.2	2.5 ± 0.8	1.6 ± 0.3	0.2 ± 0.1
Fitted multijet	0.5 ± 0.5	0.4 ± 0.4	0.07 ± 0.07	0	7.9 ± 4.5	0
MC exp. SM	44 ± 17	20 ± 8	6.7 ± 3.0	22 ± 9	79 ± 21	7.5 ± 2.5
MC exp. Top	13 ± 5	6.1 ± 2.9	1.5 ± 0.8	4.7 ± 2.2	51 ± 14	4.3 ± 1.6
MC exp. Z	22 ± 15	10 ± 7	3 ± 2	11 ± 7	7.3 ± 4.9	0.8 ± 0.8
MC exp. W	6.1 ± 4.0	2.2 ± 1.5	1 ± 1	3.5 ± 2.1	11 ± 7	2.2 ± 2.0
MC exp. Others	2.5 ± 1.0	1.4 ± 0.8	0.6 ± 0.4	2.9 ± 0.7	1.5 ± 0.4	0.2 ± 0.1
exp. multijet	0.5 ± 0.5	0.4 ± 0.4	0.07 ± 0.07	0	7.9 ± 4.5	0

Table 6: For each signal region, the observed event yield is compared with the prediction obtained from the fit. The contribution of each SM process to each signal region yield is also shown before and after the fit. The errors on the expected MC includes statistical and systematic uncertainties.

uncertainties have been taken into account for the absolute cross section production of W/Z in association with heavy flavour jets.

The uncertainty on the multijet background arises from the uncertainty in the jet response function, and it amounts to 50-100% depending on the signal region.

Finally, the uncertainty on the integrated luminosity is 3.9%.

8 Results and interpretation

Table 6 reports the number of data events observed in the each signal region, together with the SM background expectation before and after the fit. Figure 3 shows the comparison between the SM prediction and the observed data for a few relevant kinematic distributions in some of the signal regions. A SUSY sample with a relevant value of Δm between sbottom and neutralino masses is shown for reference for each signal region.

No excess above the SM expectations is observed in any of the signal regions defined. Results are used to obtain model-independent upper limits (UL) on the number of expected BSM signal events on each signal region, and on the corresponding cross section, σ_{vis}, defined as

$$\sigma_{\text{vis}} = \sigma \cdot A \cdot \varepsilon \tag{1}$$

where σ, A and ε are, respectively, the production cross section, the acceptance and the selection efficiency for a generic BSM signal. The *CLs* prescription is used to obtain 95% C.L. limits. Table 7 summarises, for each signal region, the estimated SM background yield, the observed number of events, and the expected and observed UL on event yields from a BSM signal and on σ_{vis}.

Results are interpreted in specific SUSY scenarios which assumes a SUSY particle mass hierarchy such that the sbottom decays exclusively via $\tilde{b}_1 \to b\tilde{\chi}_1^0$. Systematic uncertainties on the signal include experimental uncertainties such as JES, JER and b-tagging and are assumed to be fully correlated with those of the background. Theoretical uncertainties due to the choice of renormalisation and factorisation scales and PDF are also considered.

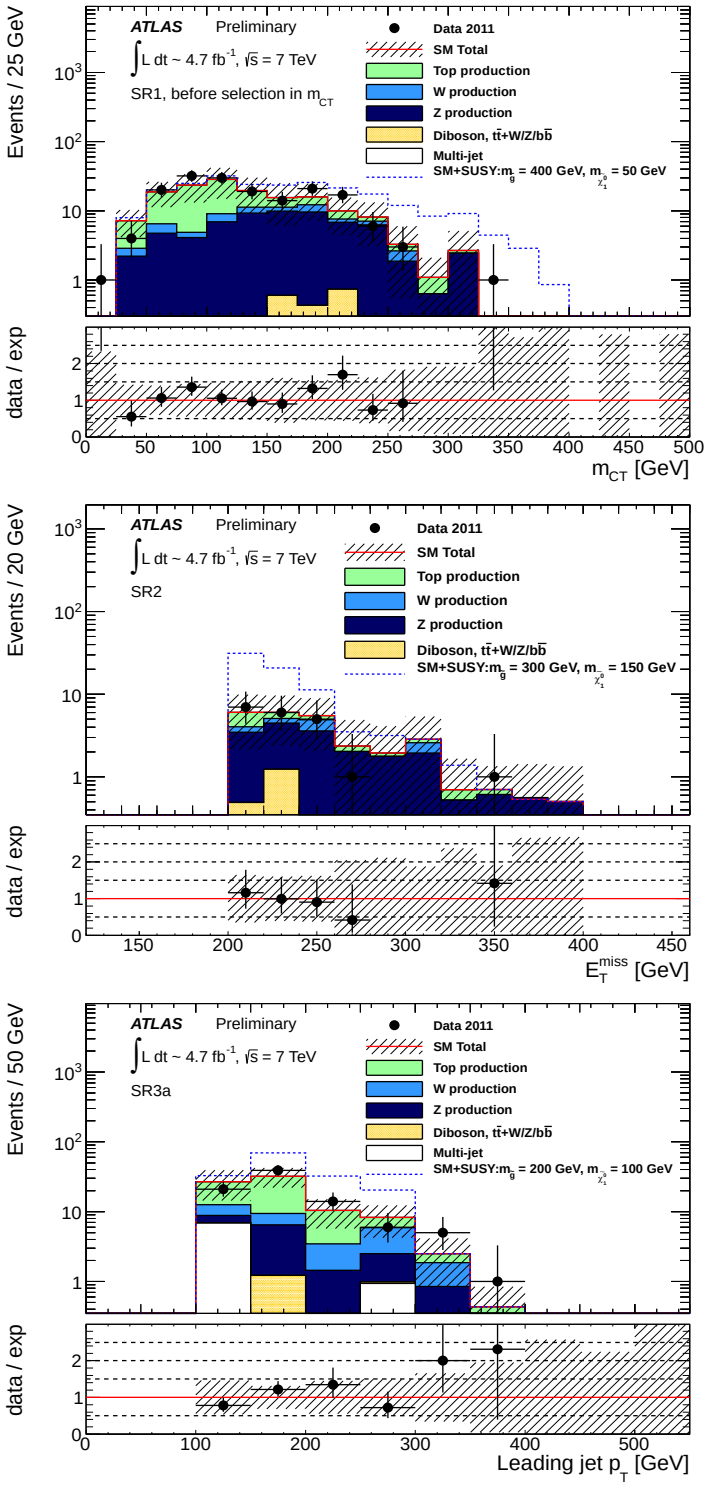

Figure 3: Top: m_{CT} distribution in SR1 before the selection on m_{CT}. Middle: $E_{\mathrm{T}}^{\mathrm{miss}}$ distribution in SR2. Bottom: leading jet p_{T} distributions in SR3. The shaded band includes both detector and theoretical systematic uncertainties. All plots are done after rescaling by the fit results.

Signal region	Background estimate	Observed data	UL on BSM event yield		UL on σ_{vis} (fb^{-1})	
			expected	observed	expected	observed
SR1 ($m_{\text{CT}} > 150$ GeV)	56 ± 11	62	25.6	28.9	5.43	6.14
SR1 ($m_{\text{CT}} > 200$ GeV)	24.9 ± 5.8	27	15.6	16.9	3.31	3.59
SR1 ($m_{\text{CT}} > 250$ GeV)	6.9 ± 2.3	4	6.94	5.22	1.47	1.11
SR2	27 ± 7	20	14.4	10.8	3.06	2.29
SR3a	81 ± 14	86	34.3	36.9	7.28	7.83
SR3b	8.0 ± 2.7	7	8.04	7.45	1.71	1.58

Table 7: Expected and observed Upper Limits (UL) on a generic BSM yield, and on $\sigma_{\text{vis}} = \sigma \cdot A \cdot \varepsilon$ for all the signal regions defined.

Figure 4 shows the exclusion limit obtained by taking in each point the signal region with the best expected *CLs* exclusion. For the MSSM scenarios considered, sbottom masses up to 490 GeV are excluded at 95% C.L. for $m_{\tilde{\chi}_1^0} = 0$. Neutralino masses up to 180 GeV are excluded for sbottom masses around 400 GeV. Sensitivity to scenarios with large Δm (> 200 GeV) is mostly obtained using the SR1 selections and, to a lesser extent SR2. The best sensitivity in the region 50 GeV$< \Delta m <$100 GeV for sbottom masses below 250 GeV is obtained with the SR3 selection. In this case, the signal acceptance depends on the MC modelling of the initial state radiation employed for the simulation of the SUSY samples. `HERWIG++` is employed for limits shown in Figure 4. Checks of the `HERWIG++` ISR modelling and its impact on the acceptance have been carried out employing alternative particle-level samples generated with `MadGraph` interfaced to `PYTHIA`. For SUSY scenarios with large splitting between sbottom and neutralino masses, differences in the kinematic acceptance are below other sources of uncertainties on the signal. For $\Delta m < 100$ GeV scenarios, an increase up to 3 times the `HERWIG++` derived acceptance is obtained using `MadGraph`+`PYTHIA` samples. This would extend the expected exclusion about 10-15 GeV in neutralino mass for sbottom masses below 300 GeV, and therefore upper limits based on `HERWIG++` signal samples are conservative.

9 Conclusions

In summary, we report results of a search for sbottom pair production in pp collisions at $\sqrt{s} = 7$ TeV, based on 4.7 fb^{-1}of ATLAS data. The events are selected with large $E_{\text{T}}^{\text{miss}}$ and two jets required to originate from b-quarks in the final state. The results are in agreement with SM predictions for backgrounds and translate into 95% C.L. upper limits on sbottom and neutralino masses in a given MSSM scenario for which the exclusive decay $\tilde{b}_1 \to b\tilde{\chi}_1^0$ is assumed. Sbottom masses up to 490 GeV are excluded for $m_{\tilde{\chi}_1^0} = 0$. Neutralino masses up to 180 GeV are excluded for sbottom masses around 400 GeV, significantly extending previous results.

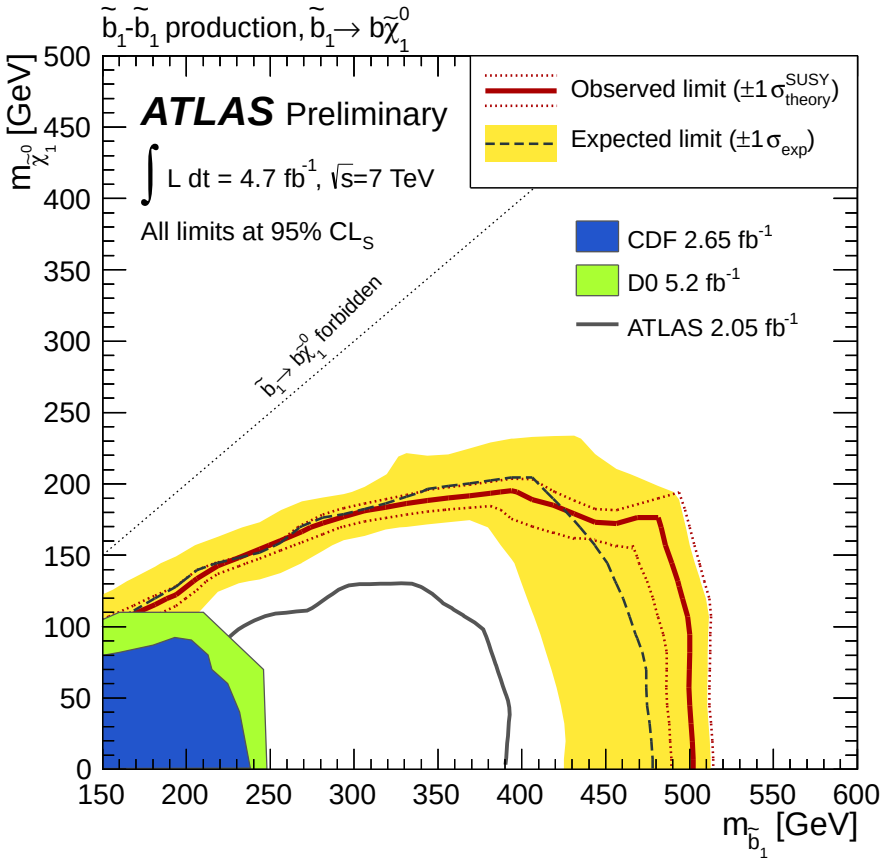

Figure 4: Expected and observed exclusion limits at 95% C.L. in the $(m_{\tilde{b}_1} - m_{\tilde{\chi}_1^0})$ obtained taking in each point the signal region which gives the best expected *CLs* exclusion. The black, dashed line shows the expected limit if theory uncertainties on the signal are neglected. The yellow band shows the $\pm 1\ \sigma$ gaussian equivalent uncertainty on the expected limit. The red solid line shows the nominal observed limit, while the red dashed lines show its variation if theory uncertainties on the signal are taken into account. Previous limits set by the ATLAS [19], CDF [60] and D0 [61] are also shown.

A Variable definitions

The following variables have been proven to be useful to reject the SM background effectively. In a given event:

$\Delta\phi_{\text{min}}(n)$: This is defined as the minimum $\Delta\phi$ between any of the leading n jets and the $\mathbf{p}_{\text{T}}^{\text{miss}}$.

$$\Delta\phi_{\text{min}} = \min(|\phi_1 - \phi_{\mathbf{p}_{\text{T}}^{\text{miss}}}|, ..., |\phi_n - \phi_{\mathbf{p}_{\text{T}}^{\text{miss}}}|) \tag{2}$$

Multi-jet events are predominantly characterised by small values of $\Delta\phi_{\text{min}}$.

m_{eff}: This is defined as the scalar sum of the p_{T} of the n jets with $p_{\text{T}} > 20$ GeV and $|\eta| < 2.8$ and the $E_{\text{T}}^{\text{miss}}$.

$$\text{m}_{\text{eff}} = \sum_{i \leq n} (p_{\text{T}}^{\text{jet}})_i + E_{\text{T}}^{\text{miss}} \tag{3}$$

where the index refers to the p_{T} ordered list of jets. This variable, used to reject QCD-multi jet background in association to the missing transverse energy, is not used as a discriminant in this analysis.

$H_{\text{T},x}$: This is the scalar sum of the p_{T} of the n jets with $p_{\text{T}} > 20$ GeV and $|\eta| < 2.8$, without including the leading x jets:

$$H_{\text{T},x} = \sum_{i=x+1}^{n} (p_{\text{T}}^{\text{jet}})_i. \tag{4}$$

The number of leading jets x excluded from this sum depends on the signal region under study.

m_{T}: This is defined using the tight lepton in the event ($p_{\text{T}}^{\text{lep}}$) and the $E_{\text{T}}^{\text{miss}}$ as follows:

$$\text{m}_{\text{T}} = \sqrt{2 p_{\text{T}}^{\text{lep}} E_{\text{T}}^{\text{miss}} - 2\vec{\mathbf{p}}_{\text{T}}^{\text{lep}} \cdot \mathbf{p}_{\text{T}}^{\text{miss}}} \tag{5}$$

This variable is used in the 1-lepton control region.

m_{CT}: The contransverse mass, m_{CT} [62], is a kinematic variable that can be used to measure the masses of pair-produced semi-invisibly decaying heavy particles. For two identical decays of heavy particles into two visible particles (or particle aggregates) v_1 and v_2, and into invisible particles, m_{CT} is defined as:

$$m_{\text{CT}}^2(v_1, v_2) = [E_{\text{T}}(v_1) + E_{\text{T}}(v_2)]^2 - [\mathbf{p}_{\text{T}}(v_1) - \mathbf{p}_{\text{T}}(v_2)]^2, \tag{6}$$

where $E_{\text{T}} = \sqrt{p_{\text{T}}^2 + m^2}$. It is an invariant quantity for decaying particles boosted back-to-back in the transverse plane. For parent particles produced with small transverse boosts, m_{CT} is bounded from above by an analytical combination of particle masses. This bound is saturated when the two visible objects are co-linear and for a given signal under consideration is given by:

$$m_{\text{CT}}^{\text{max}} = \frac{m^2(\tilde{b}) - m^2(\tilde{\chi}_1^0)}{m(\tilde{b})} \tag{7}$$

The boost-corrected contransverse mass [63] conservatively corrects rudimentary m_{CT} to account for boosts in the transverse plane due to ISR that break the invariance of the quantity. This correction ensures that the calculated m_{CT} is not smeared to higher values due to the boost from ISR and hence protects the expected endpoint in the distribution.

References

[1] H. Miyazawa, Prog. Theor. Phys. **36 (6)**, 1266 (1966)

[2] P. Ramond, Phys. Rev. **D3**, 2415 (1971)

[3] Y. Golfand, E. Likhtman, JETP Lett. **13**, 323 (1971)

[4] A. Neveu, J.H. Schwarz, Nucl. Phys. **B31**, 86 (1971)

[5] A. Neveu, J.H. Schwarz, Phys. Rev. **D4**, 1109 (1971)

[6] J. Gervais, B. Sakita, Nucl. Phys. **B34**, 632 (1971)

[7] D. Volkov, V. Akulov, Phys. Lett. **B46**, 109 (1973)

[8] J. Wess, B. Zumino, Phys. Lett. **B49**, 52 (1974)

[9] J. Wess, B. Zumino, Nucl. Phys. **B70**, 39 (1974)

[10] S. Weinberg, Phys. Rev. **D13**, 974 (1976)

[11] E. Gildener, Phys. Rev. **D14**, 1667 (1976)

[12] S. Weinberg, Phys. Rev. **D19**, 1277 (1979)

[13] L. Susskind, Phys. Rev. **D20**, 2619 (1979)

[14] P. Fayet, Phys. Lett. **B64**, 159 (1976)

[15] P. Fayet, Phys. Lett. **B69**, 489 (1977)

[16] G.R. Farrar, P. Fayet, Phys. Lett. **B76**, 575 (1978)

[17] P. Fayet, Phys. Lett. **B84**, 416 (1979)

[18] S. Dimopoulos, H. Georgi, Nucl. Phys. **B193**, 150 (1981)

[19] ATLAS Collaboration, Phys. Rev. Lett. **108**, 181802 (2012)

[20] S. Frixione, B.R. Webber, JHEP **06**, 029 (2002)

[21] S. Frixione, E. Laenen, P. Motylinski, B.R. Webber, JHEP **03**, 092 (2006)

[22] H.L. Lai, et al., Phys.Rev. **D82**, 074024 (2010)

[23] M. Mangano, et al., JHEP **07**, 001 (2003)

[24] J. Pumplin, et al., JHEP **07**, 012 (2002)

[25] G. Corcella, et al., JHEP **01**, 010 (2001)

[26] J. Butterworth, J.R. Forshaw, M. Seymour, Z. Phys. **C72**, 637 (1996)

[27] J. Alwall, M. Herquet, F. Maltoni, O. Mattelaer, T. Stelzer, JHEP **06**, 128 (2011)

[28] T. Sjöstrand, S. Mrenna, P. Skands, JHEP **05**, 026 (2006)

[29] T. Gleisberg, S. Hoeche, F. Krauss, M. Schonherr, S. Schumann, et al., JHEP **02**, 007 (2009)

[30] ATLAS Collaboration, ATLAS-CONF-2012-070 (2012), http://http://cdsweb.cern.ch/record/1460267

[31] J.M. Campbell, R.K. Ellis, Phys. Rev. **D60**, 113006 (1999)

[32] J.M. Campbell, R.K. Ellis, C. Williams, JHEP **07**, 018 (2011)

[33] J.M. Campbell, R.K. Ellis, JHEP **07**, 052 (2012)

[34] M. Garzelli, A. Kardos, C. Papadopoulos, Z. Trocsanyi, Phys.Rev. **D85**, 074022 (2012)

[35] M. Bahr, et al., Eur. Phys. J. **C58**, 639 (2008)

[36] W. Beenakker, et al., Nucl. Phys. **B515**, 3 (1998)

[37] W. Beenakker, et al., JHEP. **08**, 098 (2010)

[38] W. Beenakker, et al., Int. J. Mod. Phys. **A26**, 2637 (2011)

[39] M. Kramer, et al., arXiv:1206.2892 [hep-ph] (2012)

[40] ATLAS Collaboration, ATL-PHYS-PUB-2010-014 (2010), http://cdsweb.cern.ch/record/1277665

[41] ATLAS Collaboration, ATLAS-CONF-2010-031 (2010), http://cdsweb.cern.ch/record/1303025

[42] ATLAS Collaboration, Eur. Phys. J. **C70**, 823 (2010)

[43] S. Agostinelli, et al., Nucl. Instrum. Meth. **A506**, 250 (2003)

[44] ATLAS Collaboration, JINST **3**, S08003 (2008)

[45] ATLAS Collaboration, Eur. Phys. J. **C72**, 1909 (2012)

[46] ATLAS Collaboration, ATLAS-CONF-2011-063 (2011), http://cdsweb.cern.ch/record/1345743

[47] M. Cacciari, G. Salam, G. Soyez, JHEP **04**, 063 (2008)

[48] ATLAS Collaboration, ATLAS-CONF-2012-063 (2012), http://cdsweb.cern.ch/record/1459528

[49] ATLAS Collaboration, ATLAS-CONF-2012-053 (2012), http://cdsweb.cern.ch/record/1452641

[50] ATLAS Collaboration, arXiv:1112.6426 [hep-ex] (2011). Submitted to Eur. Phys. J. C

[51] ATLAS Collaboration, ATLAS-CONF-2012-039 (2012), http://cdsweb.cern.ch/record/1435193

[52] ATLAS Collaboration, ATLAS-CONF-2012-040 (2012), http://cdsweb.cern.ch/record/1435194

[53] ATLAS Collaboration, ATLAS-CONF-2012-043 (2012), http://cdsweb.cern.ch/record/1435197

[54] ATLAS Collaboration, arXiv:1208.0949 [hep-ex] (2012). Submitted to PRD

[55] G. Cowan, K. Cranmer, E. Gross, O. Vitells, Eur. Phys. J. **C71**, 1554 (2011)

[56] ATLAS Collaboration, Phys.Lett. **B709**, 137 (2012)

[57] ATLAS Collaboration, ATLAS-CONF-2010-054 (2010), `http://cdsweb.cern.ch/record/1281311`

[58] ATLAS Collaboration, Eur. Phys. J. **C72**, 2043 (2012)

[59] ATLAS Collaboration, ATLAS-PHYS-PUB-2011-009 (2011), `http://cdsweb.cern.ch/record/1363300`

[60] T. Aaltonen et al., CDF Collaboration, Phys. Rev. Lett. **105**, 081802 (2010)

[61] V. Abazov et al., D0 Collaboration, Phys. Lett. **B693**, 95 (2010)

[62] D. Tovey, JHEP **04**, 034 (2008)

[63] G. Polesello, D. Tovey, JHEP **03**, 030 (2010)